A DFT study of the surface charge transfer doping of diamond by chromium trioxide

Yang Xiang[1,+], Ming Jiang[1,+], Haiyan Xiao[1,*], Kaijian Xing[3], Xinxin Peng[3], Sa Zhang[1], Dongchen Qi[2,3,*]

[1]School of Physics, University of Electronic Science and Technology of China, Chengdu 610054, China

[2]School of Chemistry, Physics and Mechanical Engineering, Queensland University of Technology, Brisbane, Queensland 4000, Australia

[3]Department of Chemistry and Physics, La Trobe Institute for Molecular Science, La Trobe University, Melbourne, Victoria 3086, Australia

+ These authors contributed equally to this work.

Abstract

Hydrogen-terminated diamond surface can be rendered conductive with the formation of quasi two dimensional hole gas (2DHG) by surface acceptors through a process called surface charge transfer doping (SCTD). Recent advances in using high electron affinity transition metal oxides (e.g. MoO_3, WO_3, and V_2O_5, etc.) to achieve highly efficient and thermally stable transfer doping of diamond surface have invigorated developing robust and high-performance electronic devices based on diamond surface, whereas there lacks theoretical understanding of the underlying mechanism of SCTD and it remains unkown how the SCTD inluences the electronical and optical properties of diamond surface. In this study, we employ a density functional

theory method to investigate the surface charge transfer doping of diamond by chromium trioxide (CrO_3) with high electron affinity. Superior surface charge transfer of the hydrogenated diamond surface is demonstrated using CrO_3 as an electron acceptor. The charge density difference and bader charge reveal that the electrons are transferred from the diamond surface to CrO_3 molecule, leading to the formation of 2DHG, and the holes left in the diamond surface increase the conductivity of the diamond surface. The analysis of electronic structure indicates that high areal hole density as large as $9.83\times10^{13}cm^{-2}$ for CrO_3-doped diamond surface can be achieved. Besides, the optical absorption near infrared region of the hydrogenated diamond surface is greatly enhanced upon CrO_3 doping, which implies that this CrO_3-doped diamond surface is a promising candidate for optoelectronic materials. The present study provides an in-depth theoretical understanding of the formation of two-dimensional hole gas on diamond surface induced by a new transition metal oxide, and predicts that the CrO_3-doped diamond surface may have important implications in electronic and optoelectronic devices.

Keywords: Diamond surface; surface charge transfer doping; p-type doping; transition metal oxides; optical properties of diamond

---

* Corresponding author. E-mail address: hyxiao@uestc.edu.cn; dongchen.qi@qut.edu.au

1. Introduction

Diamond has been regarded as an technologically attractive material for a variety of electronic applications, including microwave electronic devices[1], bipolar junction transistors[2] and Schottky diodes[3], due to its many unique properties such as wide band gap, high charge carrier mobility and high thermal conductivity[4]. The combination of these properties makes diamond particularly attractive for producing high-power and high-frequency electronic devices[5]. However, development of diamond-based electronic devices has been impeded by significant technological difficulties, in particular the very high ionization energy, associated with conventional substitutional doping process[6]. Surface charge transfer doping (SCTD), which relies on charge exchange between a semiconductor and its surface dopants, offers a simple yet effective alternative to substitutional doping of diamond[7]. The SCTD model was originally proposed to explain the unexpected p-type surface conductivity that naturally occurs to air-exposed, hydrogen-terminated intrinsic diamond[8,9]. In this model, electrons are spontaneously transferred from the valence band of diamond to atmospheric adsorbates solvated in a water layer that covers diamond surface as a result of air exposure, giving rise to a subsurface two-dimensional hole gas (2DHG) and the associated p-type surface conductivity[10] with an areal hole density in the range of $10^{12} \sim 10^{13} cm^{-2}$ and a mobility around $100 cm^2 V^{-1} s^{-1}$. Exploiting this naturally occurred, air-induced surface conducting channel has thus far enabled the development of a range of field-effect transistors (FETs) that demonstrate high-power and high-frequency operations[5][11].

Despite these successes, the dependence on air-borne species and the fragile water layer to induce the surface conductivity also inevitably limits the stability and reproducibility of the resulting devices[12], greatly impacting the practical prospects of surface transfer doped diamond devices. To address these limitations, considerable research efforts have been devoted to investigating alternative molecular-type surface acceptors for the SCTD of hydrogen-terminated diamond. After that, the fullerenes (C_{60}), the fluorinated fullerenes ($C_{60}F_x$, x=18, 36 and 48) and the tetrafluoro-tetracyanoquinodimethane (F_4-TCNQ) with high electron affinity, have been also deposited on the hydrogenated diamond surface[13-16]. The first solid-state molecular surface acceptor demonstrated is fullerene C_{60} by Strobel et al. with a maximum areal hole density of $1.5\times10^{12}cm^{-2}$ [17]. Subsequently, Edmonds et al. examined the electronic properties of $C_{60}F_{48}$-doped diamond surface, and found that a high hole density close to $10^{13}cm^{-2}$ can be achieved[14]. Qi et al. have demonstrated a controllable surface transfer doping of hydrogenated diamond by the adsorption of strong electron-withdrawing molecule F_4-TCNQ, which yields a high areal hole density of about $1.6\times10^{13}cm^{-2}$ [13]. Jia et al. also studied the adsorption of F_4-TCNQ molecule on hydrogenated diamond surfaces by employing density-functional tight-binding and first-principle methods, and found that the adsorption of F_4-TCNQ induces electron transfer from the diamond surface to molecules with holes accumulating on the diamond surface[15]. However, these molecular dopants are found to be unstable at elevated temperatures, and the resulting hole densities are all lower than that of water-doped diamond surface.

In order to further enhance the hole concentration and device stability of surface transfer doped diamond, more recently the high electron affinity transition metal oxides, e.g., molybdenum oxide (MoO_3, EA=6.4 eV), tungsten trioxide (WO_3, EA=6.4 eV) and vanadium pentoxide (V_2O_5, EA=6.46 eV)[18] have been shown as highly effective surface acceptors for diamond with both sheet hole density and thermal stability superior to those of air-doped diamond[19]. The SCTD using MoO_3 was first demonstrated by Russell et al.[20] and subsequently revisited by Tordjman et al., which has a hole density exceeding $1.0\times10^{14}cm^{-2}$ [21]. Crawford et al. doped hydrogen-terminated diamond surface with V_2O_5, which exhibits superior thermal and environmental stability[22]. Tordjman et al. investigated the WO_3- and rhenium trioxide- (ReO_3) doped hydrogenated diamond surface, and found that the WO_3-doped system exhibits hole concentration of $1.7\times10^{13}cm^{-2}$ and $2.52\times10^{14}cm^{-2}$ at the temperature of 73 and 300 K, respectively, and the hole concentration for ReO_3-doped system was determined to be $2.55\times10^{13}cm^{-2}$ at 73 K and $3.63\times10^{13}cm^{-2}$ at 300 K[23]. These successes have also promoted the exploration of their device applications in FETs[24,25]. The SCTD of diamond using high electron affinity oxides therefore presents a very promising route towards the development of diamond-based surface electronics with high-performance and robust operation.

Despite these experimental advances, theoretical investigation of the SCTD of hydrogen-terminated diamond is relatively limited. Young et al. have studied the interaction between the absorbed molecules (HCl, NH_3 and H_2O) and the hydrogenated diamond surface using *ab initio* simulations, and found weak covalent interaction exists

between the H atoms of the absorbed molecules and the H atoms of the diamond surface[26]. Kim et al. employed a first-principles method to investigate the hydrogenated diamond surface with H_2O molecules, and found the surface exhibits p-type conductivity[27]. Rivero et al. have investigated the surface properties of the hydrogenated diamond surface in the presence of the NO_2, NO and O_3 molecules employing the hybrid density functional theory (DFT) method, and found that the hydrogenated C(100) surface with NO_2 dopant yields a hole density of $4.15\times10^{13}cm^{-2}$ [28]. However, a theoretical understanding of adsorption and interaction between high work function metal oxides and hydrogen-terminated diamond surface is still lacking. Furthermore, it is not clear how the presence of oxide surface acceptors will impact the electronic structures and optical properties of diamond.

In this study, we employ a DFT method to explore the structural, electronic and optical properties of hydrogenated diamond surface covered with a novel transition metal oxide surface acceptor CrO_3. The CrO_3 has an even higher electron affinity (6.75) [18,29] than that of MoO_3 or V_2O_5, and hence is expected to dope diamond more potently. Moreover, the SCTD of diamond with CrO_3 has yet been studied neither experimentally nor theoretically. In the present work, the mechanism of surface charge transfer will be investigated to efficiently control the charge redistribution between the dopant molecule and the hydrogenated diamond surface. Besides, the optical properties of the CrO_3-doped diamond surface such as absorption coefficient, reflectivity and electron energy loss spectrum of the CrO_3-doped diamond surface are calculated. The present findings may advance the experimental and theoretical studies of the diamond

surface with TMO, and open up new possibilities for superior diamond-based electronic and optoelectronic surface devices.

2. Computational Details

All calculations are carried out within the DFT framework as implemented in Vienna *Ab Initio* Simulation Package (VASP)[30-33]. The projector augmented-wave pseudopotentials are used to describe the interaction between ions and electrons, and the exchange-correlation effects are treated using the functional of Perdew–Burke–Ernzerhof (PBE) under the generalized gradient approximation (GGA)[34]. In this study, the electronic configurations for the PAW potentials are $1s^1 2s^0 2p^0$ for H, $2s^2 p^2$ for C, $2s^2 2p^4$ for O and $4s^1 4p^0 3d^5$ for Cr. The C(001):(2×1) surface is modeled by repeated slab models[35], in which one slab consists of ten carbon atomic layers and a vacuum thickness of 15 Å in the vertical direction to separate the periodically repeated slabs. The surface and bottom carbon atoms of the slab are saturated by hydrogen atoms and the CrO_3 dopant is introduced on only one side of the slab. During structural relaxation, the dopant and the atoms in the top five layers are allowed to relax while the atoms in the bottom five layers are fixed. The geometry is optimized until the total energies are less than 10^{-4} eV and the forces are smaller than 10^{-4} eV/Å. The influences of different *k*-point samplings and plane-wave cutoff energies are explored by a series of test calculations, which lead to the calculations being performed with an 8×8×1 *k*-point sampling and a cutoff energy of 450 eV.

3. Results and discussion

3.1 The structural and electronic properties of the clean hydrogen-terminated C(001)(2×1) surface

Firstly, the structural and electronic properties of the clean hydrogen-terminated diamond surface are studied. The lattice constant of the bulk diamond is calculated to be 3.57 Å, which is in excellent agreement with the experimental value of 3.57 Å[36] and other theoretical results of 3.56 Å[37]. The reconstruction of hydrogen-terminated C(001)(2×1) surface was first reported by Lurie and Wilson using low-energy electron diffraction (LEED)[38] and later reproducibly observed by Hamza et al.. These studies showed that the reconstruction of the hydrogenated C(001)(2×1) surface consists of symmetric C-C dimers, which was confirmed by several other theoretical and experimental investigations[39]. In this work, the geometrical structure of the hydrogen-terminated C(001)(2×1) surface is optimized with symmetric dimers, and the C-C dimer bond length is calculated to be 1.62 Å, which is consistent with other DFT results[40]. The band structures of the clean hydrogen-terminated C(001)(2×1) surface is also calculated (c.f. Figure 4a). The forbidden energy gap between the occupied and unoccupied surface state is determined to be 3.2 eV, which is in good agreement with the theoretical value of 3.0 eV reported by Sque et al.[41].

3.2 The adsorption configuration of CrO_3 molecule on C(001)(2×1):H surface

To understand the interaction between CrO_3 surface dopant and the hydrogen-terminated diamond surface, the energetically most favourable adsorption

configurations of individual CrO_3 molecule are firstly explored. As shown in Figure 1, three initial adsorption orientations of CrO_3 molecules, namely parallel, tilted and vertical, are considered (i.e., the normal direction of the triangular face defined by the three oxygen atoms of a CrO_3 tetrahedron is parallel, tilted and perpendicular, respectively, with respect to the diamond surface). In each case, four adsorption sites are studied, i.e., the Cr atom is located directly on top of the C site in the first layer (S1), the second layer (S2), the third layer including one directly underneath the dimer row (S3) and the other in-between dimer rows (S4), respectively. The optimized structures for the considered 12 adsorption configurations are presented in Figure 2, with the corresponding binding energies listed in Table 1. The binding energy (E_b) is defined as $E_b = E(mol) + E(surf) - E(surf + mol)$, where $E(surf + mol)$ and $E(surf)$ are the total energies of the relaxed hydrogen-terminated diamond surface with and without CrO_3 molecule, respectively, and $E(mol)$ is the total energy of relaxed CrO_3 molecule[42]. As shown in Table 1, the binding energies vary in a range of 0.25 ~ 0.56 eV for the different adsorption sites, in which the positive values are indicative of the adsorption nature of CrO_3 molecule in all considered configurations. It is noted that the binding energies of 0.55 ~ 0.56 eV for the vertical 2 (V2) and vertical 3 (V3) are notably larger than those of other configurations, suggesting that the CrO_3 molecule prefers to adsorb on diamond with the center of oxygen surface on the top of the C atoms. In the following discussions, we select V2 as the energetically most favourable configuration to discuss how the presence of CrO_3 adsorbate influences the structural, electronic and optical properties of the hydrogen-terminated diamond surface.

The structural parameters for the optimized V2 configuration are presented in Table 2, along with the initial values before adsorption for comparison. It is noted that the <Cr-O> bond length and ∠O-Cr-O bond angle increase very slightly after adsorption. The C=C dimer bond length of 1.62 Å after doping is the same as that before adsorption. The vertical distance between the CrO_3 molecule and the (001) surfaces of hydrogen-terminated diamond surface is optimized to be 1.96 Å after adsorption. The CrO_3 adsorbate also has negligible impact on the diamond layer spacing, i.e., the vertical distances between the different layers are almost unchanged after adsorption. The minimal disruption to the structures of both diamond and CrO_3 molecule indicates that there is no chemical interaction between CrO_3 and the hydrogen-terminated diamond surface, and CrO_3 molecule is physically adsorbed on the substrate, consistent with the chemically inert nature of the surface.

3.3 The electronic properties of the hydrogen-terminated C(001)(2×1) surface with CrO_3 dopant

To investigate whether charge transfer occurs between CrO_3 adsorbate and the diamond surface, the charge density difference Δρ is calculated and illustrated in Figure 3. The Δρ is computed by the formula $\Delta\rho = \rho_{\mathrm{mol+surf}} - \rho_{mol} - \rho_{surf}$, where $\rho_{mol+surf}$ is the charge density of the diamond surface with CrO_3 molecule, ρ_{mol} and ρ_{surf} are the charge densities of isolated CrO_3 molecule and the pristine hydrogen-terminated diamond surface[26], respectively. The yellow and light blue regions in Figure 3 represent electron accumulation and depletion, respectively. It can be clearly seen that

there is strong electron accumulation around the oxygen atoms of the CrO_3 molecule, whereas electron depletion appears around the surface of diamond. These results indicate that electrons are transferred from diamond surface to the CrO_3 adsorbate, leaving holes accumulating on diamond as expected from the SCTD model. To quantify the amount of charge transferred across the interface and hence the hole density on diamond, the Bader charge for the intrinsic and CrO_3 doped diamond surface is also calculated. As shown in Table 3, each CrO_3 molecule attracts about 0.36 electrons from the underlying diamond, majority of which (0.3 *e*) are transferred to the O atoms. This is consistent with the electron density plots in Figure 3. The transferred electrons mostly originate from the top layer of the diamond surface, corroborating the formation of 2DHG on diamond after CrO_3 doping. The areal hole density on diamond can be simply estimated from the amount of charge transferred per unit cell, i.e., $7.07\times10^{13}cm^{-2}$. It should also be noted that the amount of electrons gained by each CrO_3 is notably larger than that of other semiconductor systems. Xia et al. investigated the surface charge transfer of CrO_3-doped II−VI semiconductors (ZnS, ZnSe, CdS and CdSe), and found that there are 0.27 ~ 0.35 electrons transferring from the semiconductors to each CrO_3 molecule [43]. Zanella et al. studied the electronic properties of CrO_3-doped graphene layer and found that the C atoms donate 0.17 ～ 0.20 electrons to each CrO_3 molecule[44]. Our results here demonstrate that CrO_3 acts as highly efficient surface acceptors for modulating the carrier concentration and hence surface conductivity of the hole conducting channel on diamond.

The strong interfacial charge transfer as a result of the SCTD process is also

manifested by the drastic changes in the electronic structures of diamond upon the adsorption of CrO_3. The calculated band structures and (projected) density of state (DOS) distribution of diamond before and after CrO_3 adsorption are shown in Figure 4. The band structures and DOS for the CrO_3-doped diamond surface are presented in spin-up and spin-down channels in order to understand if the SCTD process induces spin polarization. As compared with the pristine diamond surface, the Fermi level of the CrO_3-doped diamond moves to the valence band edge of diamond, indicative of strong p-type degenerate doping effect of CrO_3 adsorption and the metallic character of the diamond surface, which is consistent with the charge transfer analysis presented above. In addition, the CrO_3 surface acceptor introduces a number of gap states into the diamond bandgap. More interestingly, these CrO_3-induced gap states display a clear spin-splitting, corresponding to a magnetic moment of 0.3 μ_B/per CrO_3. Such spin splitting is absent in the diamond band structures, suggesting that the induced magnetic moments mostly likely originate from transferred electrons into CrO_3 molecules. Similar spin splitting in the H_2O derived states was also observed in the system of H_2O-doped hydrogen-terminated diamond surface[45].

Further insights into the STCD process and the resulting electronic and spin properties of the doped system could be obtained from the analysis of the orbital and site projected partial DOS (PDOS). As shown in Fig. 5a, the top of valence bands for pristine hydrogen-terminated diamond consists of predominately C 2p derived states, and the top H atoms do not introduce any surface states into the bandgap, in agreement with previous reports[15]. Fig. 5b shows the PDOS of isolated CrO_3 molecule, in which

the top of the occupied states (valence band-like) are mainly comprised of O 2p-derived states, whereas the bottom of unoccupied states (conduction band-like) consist of primarily Cr 3d orbitals. Both the occupied and unoccupied states have significant Cr 3d- and O 2p- hybridization, similar to other transition metal oxides[18]. The lowest unoccupied state that is closest to the Fermi energy (labelled by the yellow arrow) will act as the acceptor state that participate in the SCTD process. There is no net magnetic moment for the CrO_3 molecule due to the completely empty 3d orbitals of Cr^{6+}. After the SCTD by CrO_3 adsorption, the Fermi level moves into the top of diamond valence band as discussed above, which also can be clearly seen in the PDOS of C atoms in Fig. 5c. Meanwhile, the original acceptor state from CrO_3 (yellow arrow) becomes partially occupied by the transferred electrons from diamond valence band. The net magnetic moment associated with the excessive electrons in CrO_3 give rise to the spin polarization in both Cr 3d and O 2p states through hybridization.

By integrating the DOS of CrO_3-doped diamond surface, the hole density is calculated to be $9.83\times10^{13}cm^{-2}$, which is larger than the value of $7.07\times10^{13}cm^{-2}$ estimated from the Bader charge. It is also noted that these results are larger than the values of $5\times10^{13}cm^{-2}$ for water molecule[46] and $4.15\times10^{13}cm^{-2}$ for NO_2 molecule[47], and comparable to highest hole densities achieved experimentally through MoO_3 and WO_3 SCTD [21,23]. Again, the CrO_3 shows great potential as a highly effective surface acceptor to realize hole density beyond $10^{14}cm^{-2}$ on diamond.

3.4 The optical properties of the hydrogen-terminated C(001)(2×1) surface with CrO_3 dopant

In order to investigate how the SCTD by CrO_3 affects the optical properties of the hydrogen-terminated diamond surface, we further calculate the absorption coefficient, reflectivity and electron energy loss function spectra of the CrO_3-doped diamond surface. The linear optical properties can be obtained from the frequency-dependent complex dielectric function

$$\varepsilon(\omega) = \varepsilon_1(\omega) + i\varepsilon_2(\omega) \quad (1),$$

where $\varepsilon_1(\omega)$ and $\varepsilon_2(\omega)$ are the real and imaginary parts of the dielectric function, respectively, and ω is the phonon energy. The imaginary part $\varepsilon_2(\omega)$ is calculated from the momentum matrix elements between the valence and conduction wave function

$$\varepsilon_2(\omega) = \frac{Ve^2}{2\pi\hbar m^2\omega^2} \times \int d^3\kappa \sum |\langle \varphi_c | p | \varphi_c \rangle|^2 \, \delta(E_c - E_v - \hbar\omega) \quad (2),$$

where V is the unit cell volume, e is the electron charge, $\hbar$ is the reduced Planck's constant, p is the momentum operator, φ_c and φ_v are the wave functions of the conduction and valence bands, respectively[48]. The real parts $\varepsilon_1(\omega)$ can then be obtained from the Kramers-Kronging relationship

$$\varepsilon_1(\omega) = 1 + \frac{2}{\pi} M \int_0^\infty \frac{\varepsilon_2(\omega')\omega'}{\omega'^2 - \omega^2} d\omega \quad (3),$$

where M is the principle value of integral[49]. The reflectivity $R(\omega)$, electron energy loss function spectra $L(\omega)$ and absorption coefficient $\alpha(\omega)$ can then be obtained from the complex dielectric function[50], i.e.,

$$n(\omega) = [\frac{\sqrt{{\varepsilon_1}^2 + {\varepsilon_2}^2} + \varepsilon_1}{2}]^{\frac{1}{2}} \quad (4),$$

$$k(\omega) = [\frac{\sqrt{{\varepsilon_1}^2 + {\varepsilon_2}^2} - \varepsilon_1}{2}]^{\frac{1}{2}} \quad (5),$$

$$R(\omega) = \frac{(n-1)^2 + k^2}{(n+1)^2 + k^2} \quad (6),$$

$$L(\omega) = \mathrm{Im}(\frac{-1}{\varepsilon(\omega)}) = \frac{\varepsilon_2}{{\varepsilon_1}^2 + {\varepsilon_2}^2} \quad (7),$$

$$\alpha(\omega) = \sqrt{2}\omega[\frac{\sqrt{{\varepsilon_1}^2 + {\varepsilon_2}^2} - \varepsilon_1}{2}]^{\frac{1}{2}} \quad (8).$$

The calculated $\varepsilon_1(\omega)$ and $\varepsilon_2(\omega)$ as a function of ω for bulk diamond is firstly calculated and presented in Figure 6, along with the experimental results for comparison[50]. For the bulk diamond, the spectrums of [100, 010, 001] crystallography orientations are degenerate, and only the results for [100] crystallography orientations are displayed in Figure 6. The calculated real-part of the dielectric function $\varepsilon_1(\omega)$ of 5.94 in the long wavelength limit (i.e. static dielectric constant) agrees well with previous experimental value of 5.82[51]. The experimental spectrum for the imaginary part of the dielectric function $\varepsilon_2(\omega)$ exhibits a threshold around 7.2 eV and a prominent peak at 12 eV due to interband transitions. It should be noted that the absorption edge corresponding to the bulk band gap of diamond of 5.5 eV is suppressed in the experimental spectrum due to its indirect transition nature. In comparison, the calculated $\varepsilon_2(\omega)$ displays a threshold at 6.0 eV and a peak around 11.5 eV, which deviate from the experimental values due to the underestimation of the band gap from DFT calculations. As for the real part of the dielectric constant, the

experimental peak at 7 eV [51] is much sharper than our calculated result due to the neglect of excitonic effects. On the other hand, the energy where ε_1 approaches to 0 eV is quite accurately found.

The calculated real and imaginary parts of dielectric function of the pristine, hydrogen-terminated and the most preferable CrO_3-doped systems are presented in Figure 7. For the pristine and the CrO_3-doped systems, the spectrums of [100, 010, 001] crystallography orientations are completely nondegenerate due to the inherent structural anisotropy. Both $\varepsilon_1(\omega)$ and $\varepsilon_2(\omega)$ display slight anisotropy character below 16 eV as expected but begin to converge at higher photon energies. The most dramatic changes to the dielectric function by CrO_3 doping are the occurrence of absorption features in $\varepsilon_2(\omega)$ at low energies well below the absorption onset of pristine diamond surface, which are related to the electronic states introduced by CrO_3 clusters (c.f. Figure 5c). The $R(\omega)$, $L(\omega)$ and $\alpha(\omega)$ of the hydrogenated diamond surface with and without CrO_3 doping are presented in Figure 8 (a), (b) and (c), respectively. The peak of the $R(\omega)$ appears at the energy of ~ 10.0 eV and the first peak of $L(\omega)$ locates at ~ 20 eV for the hydrogenated diamond surface with and without CrO_3 dopant. Overall, the changes to the reflectivity and electron energy loss function brought by the charge transfer doping are not significant. In contrast, as for the absorption spectra, the first peak of the $\alpha(\omega)$ for the CrO_3-doped diamond surface appears at ~ 1.6 eV along with other asbsorption features below the absorption onset of hydrogenated diamond surface. It is shown that the adsorption of the CrO_3 molecule on the hydrogenated diamond surface introduces new empty states within diamond band

gap, significantly enhancing the optical absorption of the Cr-doped diamond surface near infrared region. In the literature, it is also reported that the band structure of doped-system can be modified by charge transfer, thereby showing wide light absorption[52-55]. Our results suggest that the CrO_3-doped diamond surface may have great potential in the application of optoelectronic devices for infrared or near infrared light detection.

Conclusion

The structural, electronic and optical properties of the chromium trioxide- (CrO_3) doped diamond surface have been calculated by a density functional theory method. The calculations indicate that the CrO_3 molecule is physically absorbed by the substrate, and the CrO_3 dopant prefers to be stabilized on the basal (001) planes of diamond with the center of oxygen surface pointing to the C atoms. The CrO_3 dopant extracts about 0.36 electrons from the hydrogen atoms of the surface layer, resulting in the accumulation of holes on the diamond surface and the formation of quasi two-dimensional hole gas. The predicted hole density is as high as $9.83\times10^{13}cm^{-2}$ at 0 K, indicating that the CrO_3 molecule is a more promising candidate than other high work function transition metal oxides for the efficient charge transfer doping of the hydrogenated diamond surface. Besides, the CrO_3 dopant has negligible effects on the reflectivity and electron energy loss function spectrum of the hydrogenated diamond surface, whereas the optical absorption of the diamond surface near infrared region is enhanced. The present findings may advance the related experimental and theoretical investigations for the realization of superior electronic and optoelectronic devices based

on diamond surface.

Acknowledgements

H.Y. Xiao was supported by the NSAF Joint Foundation of China (Grant No. U1530129). D.C. Qi acknowledges the support of the Australian Research Council (Grant No. FT160100207). The theoretical calculations were performed using the supercomputer resources at TianHe-1 located at National Supercomputer Center in Tianjin.

References

[1] R.J. Trew, J.B. Yan, P.M. Mock, The potential of diamond and SiC electronic devices for microwave and millimeter-wave power applications, Proc. IEEE 79 (1991) 598. https://doi.org/10.1109/5.90128.

[2] M. Willander, M. Friesel, and Q. Wahab, Silicon carbide and diamond for high temperature device applications, J. Mater. Sci. 17 (2006) 1. https://doi.org/10.1007/s10854-005-5137-4.

[3] C.J.H. Wort, R.S. Balmer, Diamond as an electronic material, Mater. Today 11 (2008) 22. https://doi.org/10.1016/S1369-7021(07)70349-8.

[4] J. Isberg, et al., High carrier mobility in single-crystal plasma-deposited diamond, Science 297 (2002) 1670. https://doi.org/10.1126/science.1074374.

[5] M.J. Sear, et al., Thermal Stability and Oxidation of Group IV Terminated (100) Diamond Surfaces, Phys. Status Solidi A 215 (2018) 1800283. https://doi.org/10.1002/pssa.201800283.

[6] R. Kalish, Doping of diamond, Carbon 37 (1999) 781-785. https://doi.org/10.1016/S0008-6223(98)00270-X.

[7] W. Chen, et al., Surface transfer doping of semiconductors, Prog. Surf. Sci. 84 (2009) 279-321. https://doi.org/10.1016/j.progsurf.2009.06.002.

[8] M.I. Landstrass, K.V. Ravi, Resistivity of chemical vapor deposited diamond films, Appl. Phys. Lett. 55 (1989) 975. https://doi.org/10.1063/1.101694.

[9] M.I. Landstrass, K.V. Ravi, Hydrogen passivation of electrically active defects in diamond, Appl. Phys. Lett. 55 (1989) 1391. https://doi.org/10.1063/1.101604.

[10] F. Maier, et al., Origin of Surface Conductivity in Diamond, Phys. Rev. Lett. 85 (2000) 3472-3475. https://doi.org/10.1103/PhysRevLett.85.3472.

[11] C.I. Pakes, J.A. Garrido, and H. Kawarada, Diamond surface conductivity: Properties, devices and sensors, MRS Bulletin, 39 (2014) 542-548. https://doi.org/10.1557/mrs.2014.95.

[12] M. Kasu, et al., Diamond-based RF power transistors: Fundamentals and applications, Diam. Relat. Mater. 16 (2007) 1010-1015. https://doi.org/10.1016/j.diamond.2006.12.046.
[13] D.C. Qi, et al., Surface Transfer Doping of Diamond (100) by Tetrafluoro-tetracyanoquinodimethane, J. Am. Chem. Soc. 129 (2007) 8084. https://doi.org/10.1021/ja072133r.
[14] M.T. Edmonds, et al., Surface transfer doping of hydrogen-terminated diamond by $C_{60}F_{48}$: energy level scheme and doping efficiency, J. Chem. Phys. 136 (2012) 124701. https://doi.org/10.1063/1.3695643.
[15] G.X. Jia, et al., Adsorptions of Tetrafluorotetracyanoquinodimethane on Entirely and Partially Hydrogenated C(100)-2x1 Surfaces, J. Phys. Chem. C. 113 (2009) 8829. https://doi.org/10.1021/jp9000187.
[16] D.P. Langley, et al., Surface transfer doping of diamond with a molecular heterojunction, Appl. Phys. Lett. 100 (2012) 032103. https://doi.org/10.1063/1.3676445.
[17] P. Strobel , M. Riedel, J. Ristein, Surface transfer doping of diamond. Nature 430 (2004) 439. https://doi.org/10.1038/nature02751.
[18] M.T. Greiner, Universal energy-level alignment of molecules on metal oxides, Nat. Mater. 11 (2012) 76-80. https://doi.org/10.1038/nmat3159.
[19] C. Verona, et al., Comparative investigation of surface transfer doping of hydrogen terminated diamond by high electron affinity insulators, J. Appl. Phys. 120 (2016) 025104. https://doi.org/10.1063/1.4955469.
[20] S.A.O. Russell, et al., Surface transfer doping of diamond by MoO_3: A combined spectroscopic and Hall measurement study, Appl. Phys. Lett. 103 (2013) 202112. https://doi.org/10.1063/1.4832455.
[21] M. Tordjman, et al., Superior Surface Transfer Doping of Diamond with MoO_3. Adv. Mater. Interface 1 (2014) 1300155. https://doi.org/10.1002/admi.201300155.
[22] K.G. Crawford, et al., Enhanced surface transfer doping of diamond by V_2O_5 with improved thermal stability, Appl. Phys. Lett. 108 (2016) 042103. https://doi.org/10.1063/1.4940749.
[23] M. Tordjman, K. Weinfeld, R. Kalish, Boosting surface charge-transfer doping efficiency and robustness of diamond with WO_3 and ReO_3, Appl. Phys. Lett. 111 (2017) 111601. https://doi.org/10.1063/1.4986339.
[24] Z. Yin, et al., A Diamond:H/WO_3 Metal–Oxide–Semiconductor Field-Effect Transistor, IEEE Electron Device Letters. 39 (2018) 540-543. https://doi.org/10.1109/LED.2018.2808463.
[25] Z.Y. Yin, et al., Enhanced transport in transistor by tuning transition-metal oxide electronic states interfaced with diamond, Sci. Adv. 4 (2018) 1-10. https://doi.org/10.1126/sciadv.aau0480.
[26] H.X. Young, Y. Yu, L.F. Xu, C.Z. Gu, Ab initio study of molecular adsorption on hydrogenated diamond (001) surfaces, Journal of Physics: Conference Series 29 (2006) 145. https://doi.org/10.1088/1742-6596/29/1/027.
[27] Y.H. Kim, S.B. Zhang, Y. Yu, L.F. Xu, C.Z. Gu, Dihydrogen bonding, p-type conductivity, and origin of change in work function of hydrogenated diamond (001) surfaces, Phys. Rev. B 74 (2006) 075329. https://doi.org/10.1103/PhysRevB.74.075329.
[28] P. Rivero, W. Shelton, V. Meunier, Surface properties of hydrogenated diamond in the presence of adsorbates: A hybrid functional DFT study, Carbon 110 (2016) 469-79. https://doi.org/10.1016/j.carbon.2016.09.050.
[29] B.D. Pelatt, et al., Atomic solid state energy scale: Universality and periodic trends in oxidation

state, J. Solid State Chem. 231 (2015) 138-144. https://doi.org/10.1016/j.jssc.2015.07.037.
[30] G. Kresse, J. Furthmüller, Efficient iterative schemes for ab initio total-energy calculations using a plane-wave basis set, Phys. Rev. 54 (1996) 11169. https://doi.org/10.1103/PhysRevB.54.11169.
[31] G. Kresse, J. Furthmüller, Efficiency of ab-initio total energy calculations for metals and semiconductors using a plane-wave basis set, Comput. Mater. Sci. 6 (1996) 15. https://doi.org/10.1016/0927-0256(96)00008-0.
[32] G. Kresse, D. Joubert, From ultrasoft pseudopotentials to the projector augmented-wave method, Phys. Rev. B 59 (1999) 1758. https://doi.org/10.1103/PhysRevB.59.1758.
[33] P.E. Blöchl, Projector augmented-wave method, Phys. Rev. B 50 (1994) 17953. https://doi.org/10.1103/PhysRevB.50.17953.
[34] J.P. Perdew, L. Burke, M. Ernzerhof, Generalized Gradient Approximation Made Simple, Phys. Rev. Lett. 77 (1996) 3865. https://doi.org/10.1103/PhysRevLett.77.3865.
[35] H.Y. Xiao, X.T. Zu, Y.F. Zhang, L. Yang, First-principles study of the adsorption of cesium on Si(001)(2x1) surface, J. Chem. Phys. 122 (2005) 174704. https://doi.org/10.1063/1.1886733.
[36] X. Liu, C. Kang, H. Qiao, Y. Ren, X. Tan, S. Sun, Theoretical Studies of the Adsorption and Migration Behavior of Boron Atoms on Hydrogen-Terminated Diamond (001) Surface, Coatings 7 (2017) 57. https://doi.org/10.3390/coatings7050057.
[37] X. Y. Cui, D. Ying, Bai Biao H. DFT study of halogen impurity in diamond, J. Phys. D Appl. Phys. 42 (2009) 145407. https://doi.org/10.1088/0022-3727/42/14/145407.
[38] T. Takashi, I. Takahiro, N. Yoshiki, H. Kotaro, F. Naoji, Epitaxially Grown Diamond (001) 2×1/1×2 Surface Investigated by Scanning Tunneling Microscopy in Air, Jap. J. Appl. Phys. 30 (1991) 1063. https://doi.org/10.1143/jjap.30.1063.
[39] H. Kawarada, H. Sasaki, A. Sato, Scanning-tunneling-microscope observation of the homoepitaxial diamond (001) 2x1 reconstruction observed under atmospheric pressure, Phys. Rev. B 52 (1995) 11351-8. https://doi.org/10.1103/PhysRevB.52.11351.
[40] Y. Yu, C.Z. Gu, L.F. Xu, S.B. Zhang, Ab initio structural characterization of a hydrogen-covered diamond (001) surface, Phys. Rev. B 70 (2004) 125423. https://doi.org/10.1103/PhysRevB.70.125423.
[41] S.J. Sque, R. Jones, P.R. Briddon, Structure, electronics, and interaction of hydrogen and oxygen on diamond surfaces, Phys. Rev. B 73 (2006) 085313. https://doi.org/10.1103/PhysRevB.73.085313.
[42] S.B. Gesari, M.E. Pronsato, A. Visintin, A. Juan, Hydrogen Storage in AB_2 Laves Phase (A = Zr, Ti; B = Ni, Mn, Cr, V): Binding Energy and Electronic Structure, J. Phys. Chem. C 114 (2010) 16832-6. https://doi.org/10.1021/jp106036v.
[43] F. Xia, Z. Shao, Y. He, R. Wang, X. Wu, T. Jiang, et al. Surface Charge Transfer Doping via Transition Metal Oxides for Efficient p-Type Doping of II-VI Nanostructures, ACS Nano 10 (2016) 10283-93. https://doi.org/10.1021/acsnano.6b05884.
[44] I. Zanella, S. Guerini, S.B. Fagan, J. Mendes, A.G. Souza Chemical doping-induced gap opening and spin polarization in graphene, Phys. Rev. B 77 (2008) 073404. https://doi.org/10.1103/PhysRevB.77.073404.
[45] O. Manelli, S. Corni, M.C. Righi, Water Adsorption on Native and Hydrogenated Diamond (001) Surfaces, J. Phys. Chem. C. 114 (2010) 7045-53. https://doi.org/10.1021/jp910971e.

[46] C. Sauerer, F. Ertl, C.E. Nebel, M. Stutzmann, P. Bergonzo, O.A. Williams, et al. Low Temperature Surface Conductivity of Hydrogenated Diamond, Phys. Status Solidi A 186 (2001) 241-7. https://doi.org/10.1002/1521-396X(200108)186:2<241::AID-PSSA241>3.0.CO;2-1.
[47] P. Rivero, W. Shelton, V. Meunier, Surface properties of hydrogenated diamond in the presence of adsorbates: A hybrid functional DFT study, Carbon 110 (2016) 469-79. https://doi.org/10.1016/j.carbon.2016.09.050.
[48] H. Ehrenreich, M.H. Cohen, Self-Consistent Field Approach to the Many-Electron Problem, Phys. Rev. 115 (1959) 786-90. https://doi.org/10.1103/PhysRev.115.786.
[49] M. Dressel, B. Gompf, D. Faltermeier, A.K. Tripathi, J. Pflaum, M. Schubert, Kramers-Kronig-consistent optical functions of anisotropic crystals: generalized spectroscopic ellipsometry on pentacene, Opt Express 16 (2008) 19770-8. https://doi.org/10.1364/OE.16.019770.
[50] Z. Cui, X. Ke, E. Li, T. Liu, Electronic and optical properties of titanium-doped GaN nanowires, Mater. Design 96 (2016) 409-15. https://doi.org/10.1016/j.matdes.2016.02.050.
[51] H.R. Philipp, E.A. Taft, Optical Properties of Diamond in the Vacuum Ultraviolet, Phys. Rev. 127 (1962) 159. https://doi.org/10.1103/PhysRev.127.159.
[52] C.Y. Zhou, D.L. Huang, P. Xu, et al. Efficient visible light driven degradation of sulfamethazine and tetracycline by salicylic acid modified polymeric carbon nitride via charge transfer, Chem. Eng. J. 370 (2019) 1077-1086. https://doi.org/10.1016/j.cej.2019.03.279.
[53] C.Y. Zhou, C. Lai, P. Xu, et al. Rational design of carbon-doped carbon nitride/$Bi_{12}O_{17}Cl_2$ composites: a promising candidate photocatalyst for boosting visible-light-driven photocatalytic degradation of tetracycline, ACS Sustainable Chem. Eng. 6(5) (2018) 6941-6949. https://doi.org/10.1021/acssuschemeng.8b00782.
[54] C.Y. Zhou, C. Lai, D.L. Huang, et al. Highly porous carbon nitride by supramolecular preassembly of monomers for photocatalytic removal of sulfamethazine under visible light driven, Appl. Catal., B 220 (2018) 202-210. https://doi.org/10.1016/j.apcatb.2017.08.055.
[55] C.Y. Zhou, P. Xu, C. Lai, et al. Rational design of graphic carbon nitride copolymers by molecular doping for visible-light-driven degradation of aqueous sulfamethazine and hydrogen evolution, Chem. Eng. J. 359 (2019) 186-196. https://doi.org/10.1016/j.cej.2018.11.140.

Table 1. The calculated binding energies for the different CrO_3-doped diamond surfaces. The corresponding configurations are illustrated in Figure 1.

Configuration	Binding energy (eV)			
	1	2	3	4
Parallel doping	0.25	0.32	0.32	0.41
Tilted doping	0.50	0.39	0.28	0.15
Vertical doping	0.49	0.56	0.55	0.36

Table 2. The optimized structural parameters of the pristine and the CrO_3-doped diamond surfaces. d: the bond length between atoms; Δ d: the vertical distance between layers.

Structural parameters	before adsorption	after adsorption
d<Cr-O> (Å)	1.61/1.61/1.61	1.62/1.62/1.62
∠O-Cr-O (°)	112/112/112	113/113/113
d <C=C dimer> (Å)	1.62	1.62
Δ d (CrO_3 -H layer) (Å)	-	1.96
Δ d (H layer -First C layer) (Å)	1.01	1.01
Δ d (First C layer-Second C layer) (Å)	0.81	0.81
Δ d (Second C layer -Third C layer) (Å)	0.80	0.80
Δ d (Third C layer -Fourth C layer) (Å)	0.93	0.93

Table 3. The calculated Bader charges for the CrO_3-doped diamond surface.

	Bader charge (|e|)	
	before adsorption	after adsorption
Diamond: H	0	0.36
CrO_3	0	-0.36
Cr	1.78	1.72
O	-1.78	-2.08
surface H layer	0	0.45
the first C layer	-0.11	-0.20
the second C layer	-0.01	-0.04
the third C layer	0.14	0.13
bottom H layer	-0.05	-0.01

Figure captions

Figure 1. Schematic view of the considered configurations for CrO_3-doped diamond surface. For parallel, tilted and vertical doping, the normal direction of the three-oxygen surface is parallel, tilted and perpendicular to the diamond surface, respectively. The Cr atom is located directly on top of the C site in the first layer (S1), the second layer (S2), the third layer included one directly underneath the dimer row (S3) and the other in-between dimer rows (S4). The dark blue, red, brown and light blue spheres represent Cr, O, C and H atoms, respectively.

Figure 2. Schematic view of the optimized structures for the considered configurations of CrO_3-doped diamond surface.

Figure 3. The (a) side-view and (b) top-view of charge density differences for the most preferable CrO_3-doped diamond surface. The yellow and light blue regions represent the electron accumulation and depletion, respectively. The isosurface values are 0.001 e/Å^3.

Figure 4. The band structures of (a) clean hydrogenated diamond surface and (b) the most preferable CrO_3-doped diamond surface. The fermi energy is located at 0 eV.

Figure 5. Partial density of state (PDOS) distribution of (a) the clean hydrogenated diamond surface, (b) the CrO_3 molecule and (c) CrO_3-doped diamond surface. The E_F is fermi energy.

Figure 6. (a) Real part $\varepsilon_1(\omega)$ and (b) imaginary part $\varepsilon_2(\omega)$ of the calculated dielectric constant for bulk diamond compared to experimental results[50].

Figure 7. The dielectric function of (a) real part $\varepsilon_1(\omega)$ and (b) imaginary part $\varepsilon_2(\omega)$

for the clean hydrogenated diamond surface and the most preferable CrO_3-doped diamond surface.

Figure 8. The comparison of the optical properties for the clean hydrogenated diamond surface and the most preferable CrO_3-doped diamond surface: (a) the reflectivity spectrum ($R(\omega)$); (b) the electron energy loss function spectrum ($L(\omega)$) and (c) the absorption coefficient spectrum ($\alpha(\omega)$).

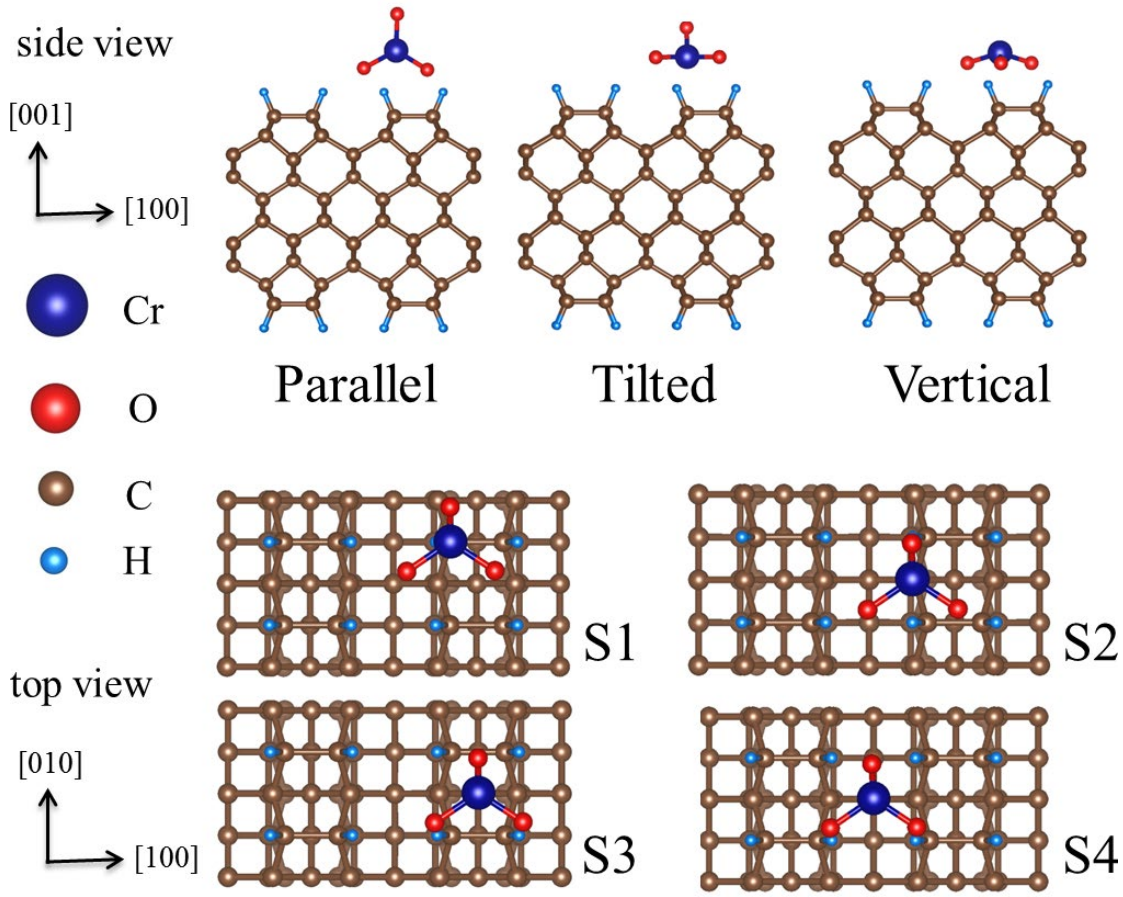
side view
[001]
[100]
Cr
O
C
H
Parallel
Tilted
Vertical
S1
S2
top view
[010]
[100]
S3
S4

Figure 1

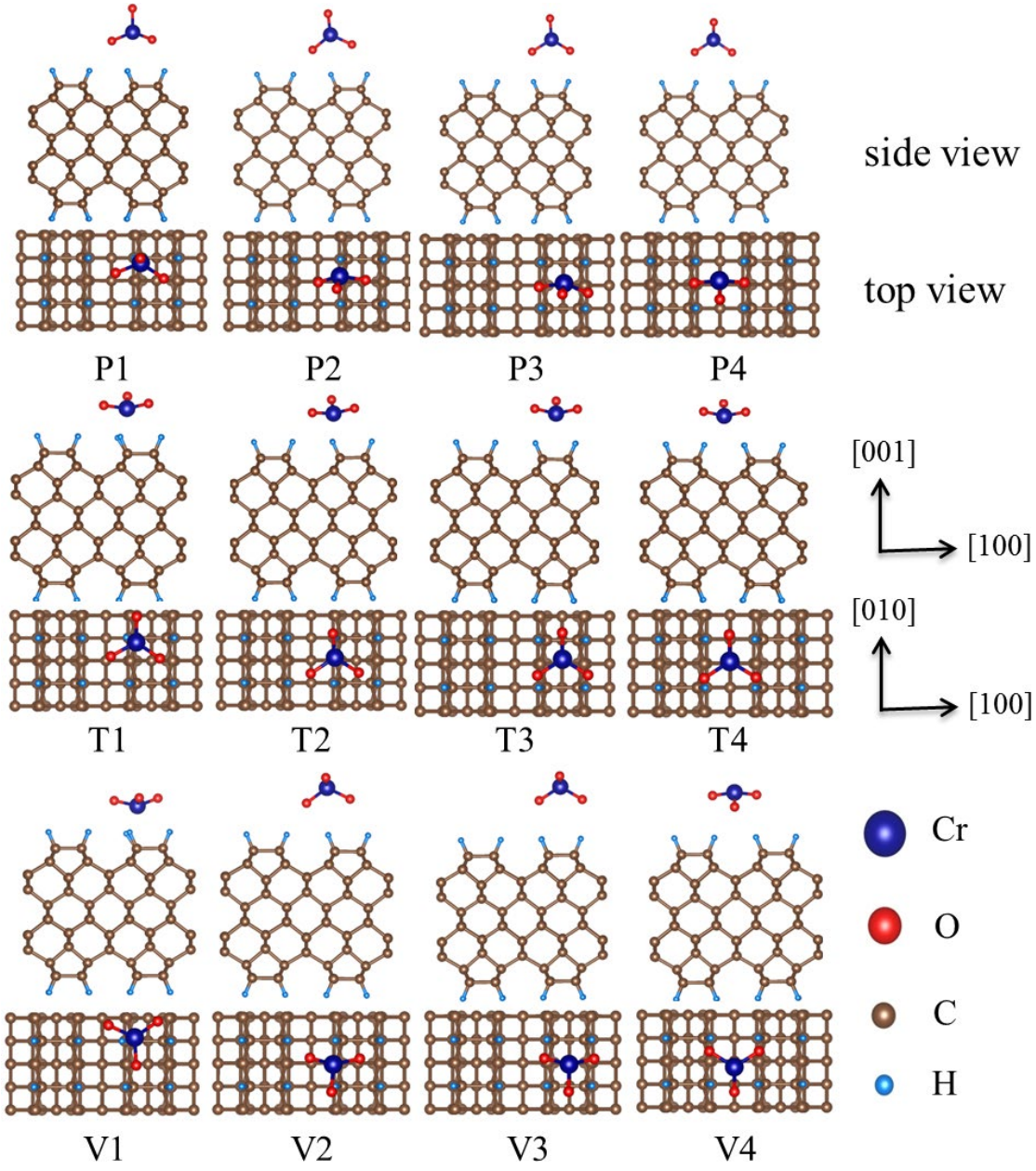
side view
top view
P1
P2
P3
P4
[001]
[100]
[010]
[100]
T1
T2
T3
T4
Cr
O
C
H
V1
V2
V3
V4

Figure 2

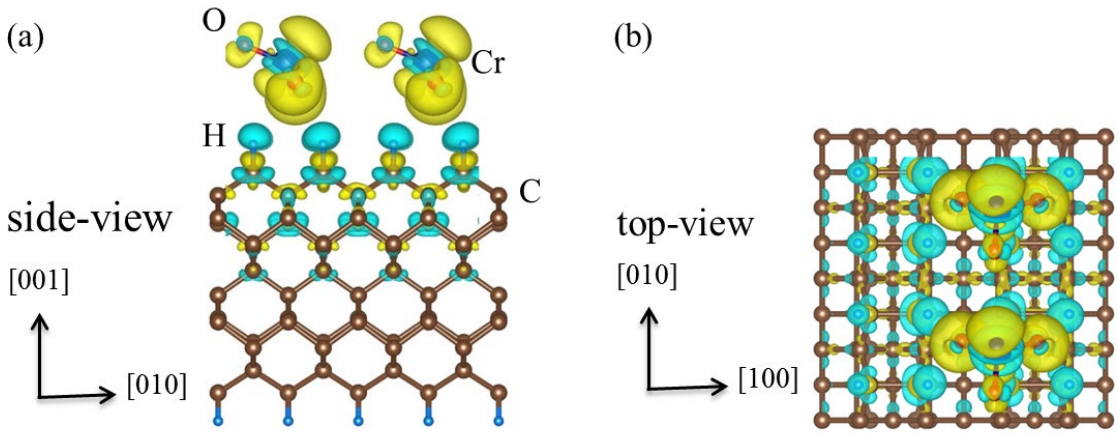

Figure 3

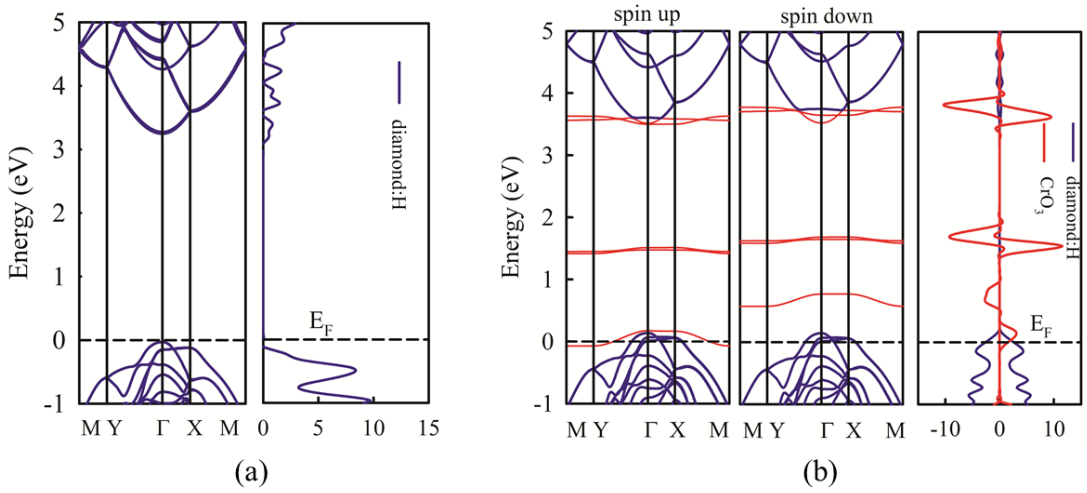
Energy (eV)
5
4
3
2
1
0
-1
M Y Γ X M
0 5 10 15
diamond:H
E_F
(a)
spin up
spin down
M Y Γ X M M Y Γ X M
-10 0 10
CrO3
diamond:H
E_F
(b)

Figure 4

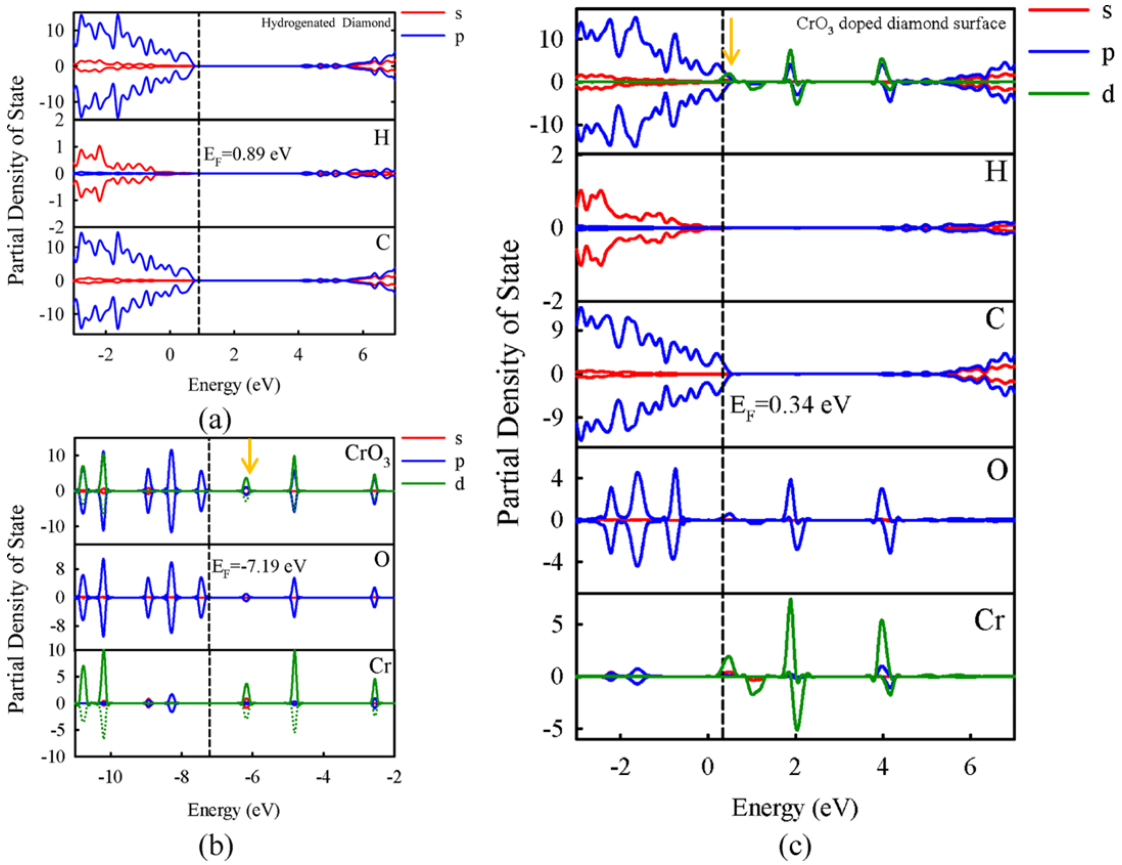
Hydrogenated Diamond
H
C
E_F=0.89 eV
Partial Density of State
Energy (eV)
(a)
s
p
d
CrO_3
O
Cr
E_F=-7.19 eV
Partial Density of State
Energy (eV)
(b)
CrO_3 doped diamond surface
H
C
O
Cr
E_F=0.34 eV
Partial Density of State
Energy (eV)
(c)

Figure 5

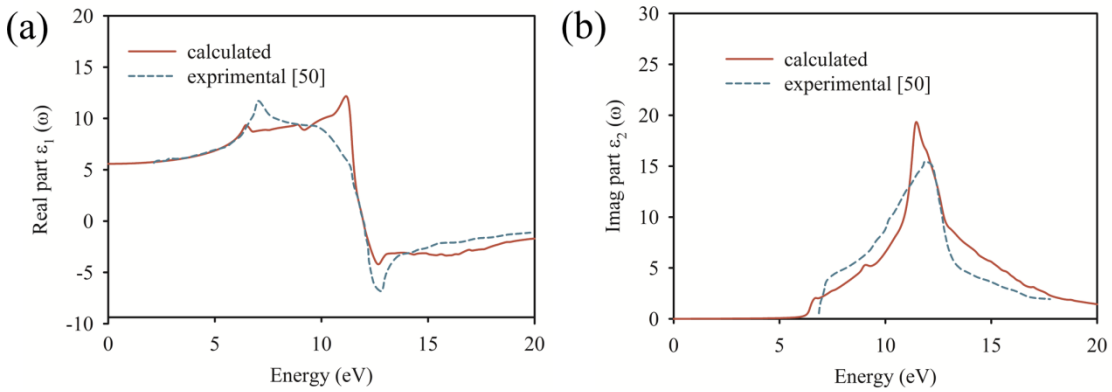
(a)
calculated
exprimental [50]
Real part ε_1 (ω)
Energy (eV)
(b)
calculated
experimental [50]
Imag part ε_2 (ω)
Energy (eV)

Figure 6

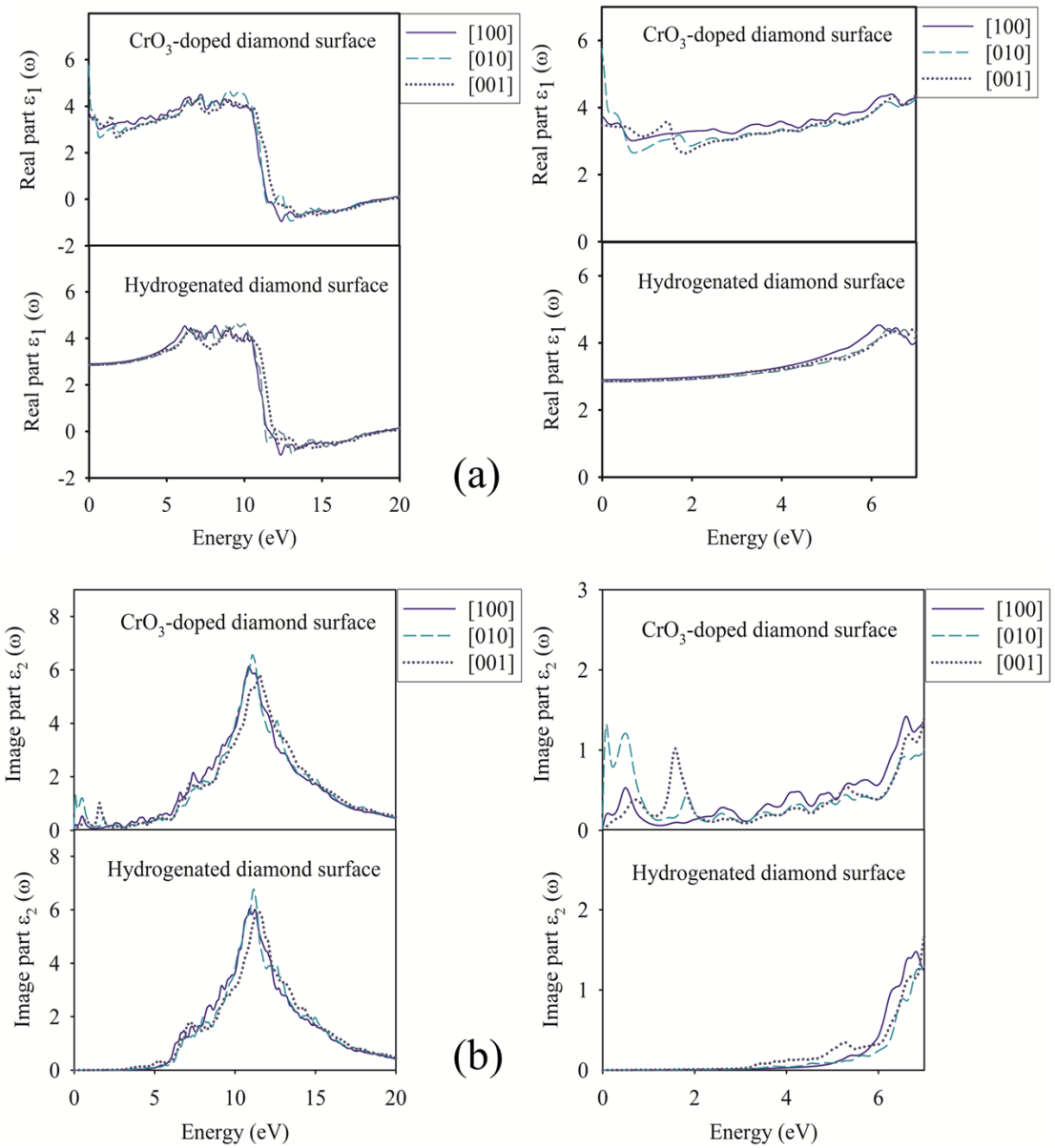
CrO3-doped diamond surface
Hydrogenated diamond surface
[100]
[010]
[001]
Real part ε1 (ω)
Image part ε2 (ω)
Energy (eV)
(a)
(b)

Figure 7

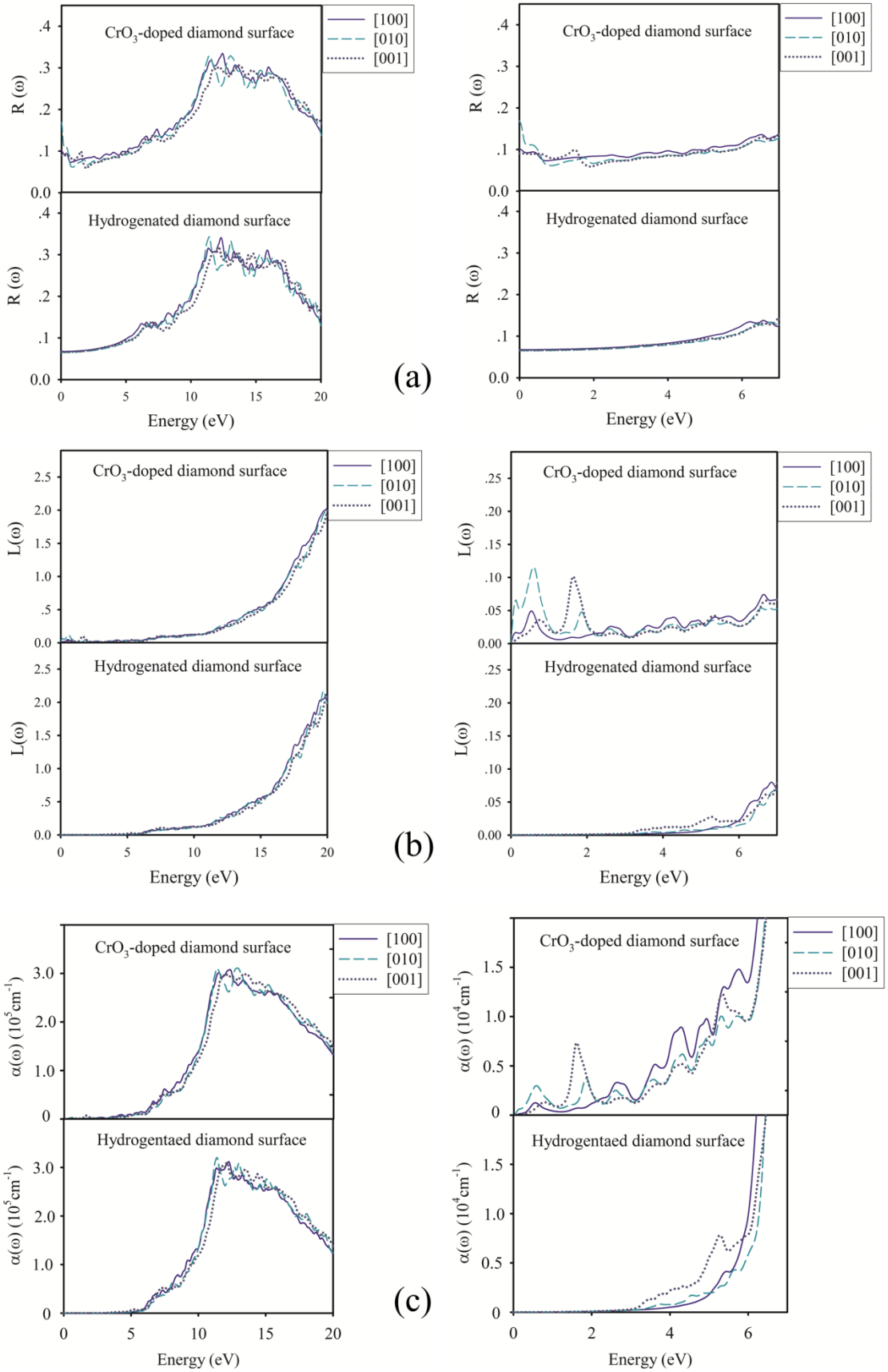
CrO3-doped diamond surface
Hydrogenated diamond surface
[100]
[010]
[001]
R (ω)
L(ω)
α(ω) (10^5cm^-1)
α(ω) (10^4cm^-1)
Energy (eV)
(a)
(b)
(c)

Figure 8